Observer-Pattern Modeling and Nonlinear Modal Analysis of Two-Stage Boost Inverter

Hao Zhang, *Member, IEEE*, Weijie Li, Honghui Ding, Chuanzhi Yi, and Xiaojin Wan

***Abstract*—This paper deals with modeling and nonlinear modal analysis of two-stage boost inverter. An observer-pattern modeling method is proposed to eliminate the time-variance effect from both fundamental component in the load stage and "hidden" second-harmonic one in the source stage. Then, based on the observer-pattern model, the nonlinear modal analysis method is applied to obtain a closed-form analytical representation of the nonlinear system, which yields a great deal of physical insight into the system dynamics. First, fundamental modal analysis is calculated to indicate the correlation between fundamental modes, state variables, and circuit parameters. Such key parameters as C_1 and T_3 are found to be beneficial to the dynamical performance of the whole system. Second, the second-order nonlinear interaction indices are proposed to uncover the underlying mechanism of nonlinear interaction behaviors, and the relationship between modal interaction and system parameters is explored quantitatively. Finally, theoretical analysis is verified by circuit experiments. These results are beneficial to the improvement of transient performance as well as the understanding of the nonlinear interactions in transient behavior.**

***Index Terms*—Hidden second harmonics, nonlinear modal analysis, observer-pattern modeling, second-order interacted mode, two-stage boost inverter.**

I. Introduction

With the rapid development of industrial technology, the power system is now faced with two main serious challenges: higher power quality, and particularly stricter reliability. Due to some considerable advantages such as step-down and step-up voltage operation, continuous input current, and lower input current ripple, two-stage boost inverter becomes one of the most attractive and viable solutions to the power conversion problem, i.e., the control of the power flow from dc to ac, and are gaining increased acceptance in many applications such as photovoltaic array and servo-motor drive [1]. In actual applications, the two-stage system can inevitably suffer from a variety of disturbances such as start-up procedure, circuit topology fault, and sudden load jump [2]–[4], which may result in degrading the efficiency of systems, threatening the safe operation of cascade converters and even making the system collapse during the transient process [5], [6]. Therefore, it is always desirable to deepen the understanding of the transient interaction behavior ahead in practical engineering.

Together with the system stability, plenty of investigations have been carried out into the transient behaviors of two-stage system in the past several decades [7]–[15]. Since the seminal work of Middlebrook [16], linearized analysis approach has become one simple, yet powerful tool to analyze the stability and transient characteristics of two-stage dc–dc converters [17], [18]. Actually, if this impedance criterion is satisfied, then the two-stage system can be decoupled, i.e., the interaction among subsystems can be ignored [19]. Subsequently, many researchers have devoted themselves to modifying the Middlebrook impedance criterion [17], [20]. For instance, Wildrick [21] and Feng *et al*. [22] proposed a forbidden region method to satisfy the requirement of the system stability margin, which can be used to analyze the system-level stability and transient behaviors because the linear interactions between the two subsystems are considered carefully. On the other hand, for the purpose of simplifying the control loop design of the source-stage converter, the input impedance of a tightly controlled load-stage converter had been usually approximately characterized as a negative resistor in small-signal SPICE circuit [19], [20]. However, in practical engineering, those results frequently gave no reasonable explanations for some transient phenomena. One main reason is that the linearized approach only reserves linear dynamical information but loses plenty of nonlinear interacted dynamical information, which is just responsible for the transient behaviors. In fact, different from two-stage dc–dc converter, the two-stage boost inverter has the "hidden" second-harmonic component at the input of the downstream H-bridge inverter because of the effect of the nonlinear interactions between the source stage and load stage [1], [23]–[25], which leads to a great deal of trouble in both system modeling and interaction analysis. Even if the bifurcation analysis method is widely used to analyze nonlinear behaviors of power switching converters [12], [15], [26], [28], the nonlinear method cannot evaluate the transient interaction behavior at all. This reason is that the bifurcation method has some good advantages in the long-term stability and dynamical evolution rather than such short-term dynamics as transient behavior [13], [27]–[30]. This becomes another barrier. Therefore, until now, the mechanism of the nonlinear transient interaction has not been explored clearly as yet.

In this paper, an observer-pattern modeling method will be proposed to eliminate the effect of time variance originated from

Manuscript received March 29, 2017; revised August 3, 2017; accepted September 14, 2017. Date of publication September 25, 2017; date of current version April 20, 2018. This work was supported by the National Natural Science Foundation of China under Grants 51577141 and 61571357. Recommended for publication by Associate Editor C. K. Tse. *(Corresponding author: Hao Zhang.)*

The authors are with the State Key Lab of Electrical Insulation & Power Equipment, School of Electrical Engineering, Xi'an Jiaotong University, Xi'an 710049, China (e-mail: haozhang@xjtu.edu.cn; liweijie883@163.com; dinghonghui@stu.xjtu.edu.cn; yichuanzhi1@outlook.com; wanjiajin@stu.xjtu.edu.cn).

Color versions of one or more of the figures in this paper are available online at http://ieeexplore.ieee.org.

Digital Object Identifier 10.1109/TPEL.2017.2756090

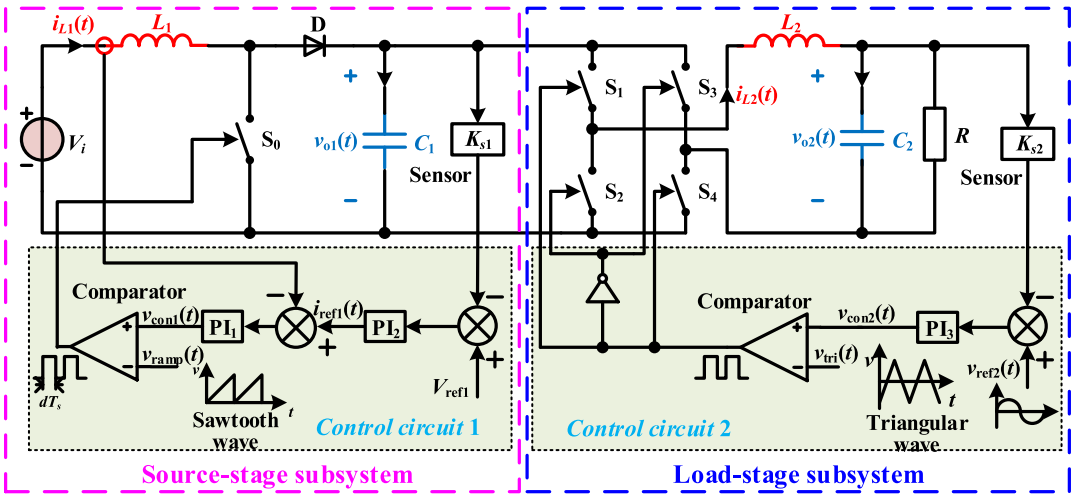

Fig. 1. Schematic diagram of the two-stage boost inverter.

both fundamental component and "hidden" second-harmonic component in the derived averaged equations of the two-stage boost inverter. Then, nonlinear modal analysis method will be adopted to obtain a closed-form approximate solution for the observer-pattern model. First, the fundamental modal sensitivity and contribution factor will be calculated to indicate the relationship among state variables, fundamental modes, and circuit parameters. Second, second-order nonlinear interaction indices will be proposed to quantify the nonlinear effect on system dynamical characteristics and the effect of system parameters on modal interactions will be investigated to reveal the mechanism of the dynamical characteristics. Finally, some experiment results will be provided to verify the theoretical analysis.

II. System Description and Nonlinear Averaged Equations

A. Operation Principle

The two-stage boost inverter consists of a boost dc–dc source-stage converter and an H-bridge load-stage inverter, as shown in Fig. 1. In the source-stage converter, an average-current-mode controller is employed to ensure the fast dynamic response. The reference current $i_{\mathrm{ref1}}(t)$ and the control signal $v_{\mathrm{con1}}(t)$ can be written as

$$i_{\mathrm{ref1}}(t) = K_1[V_{\mathrm{ref1}} - K_{\mathrm{s1}}v_{\mathrm{o1}}(t)] + \frac{K_1}{T_1}\int_0^t [V_{\mathrm{ref1}} - K_{\mathrm{s1}}v_{\mathrm{o1}}(\tau)]d\tau \tag{1}$$

$$v_{\mathrm{con1}}(t) = K_2[i_{\mathrm{ref1}} - i_{L1}(t)] + \frac{K_2}{T_2}\int_0^t [i_{\mathrm{ref1}} - i_{L1}(\tau)]\mathrm{d}\tau \tag{2}$$

where K_{s1} is the sampling coefficient of the source-stage voltage sensor, K_k and T_k $(k = 1, 2)$ are the proportional coefficient and integral coefficient, respectively.

The sawtooth ramp signal $v_{\mathrm{ramp}}(t)$ is given by

$$v_{\mathrm{ramp}}(t) = V_{m1}\frac{t \bmod T_{s1}}{T_{s1}} \tag{3}$$

where T_{s1} is the switching period and V_{m1} is the amplitude of $v_{\mathrm{ramp}}(t)$.

The voltage-mode controller is adopted in the load-stage inverter. The expression for the control signal $v_{\mathrm{con2}}(t)$ is

$$v_{\mathrm{con2}}(t) = K_3[v_{\mathrm{ref2}}(t) - K_{s2}v_{o2}(t)] + \frac{K_3}{T_3}\int_0^t [v_{\mathrm{ref2}}(\tau) - K_{s2}v_{o2}(\tau)]\mathrm{d}\tau \tag{4}$$

where K_3 is the proportional coefficient, T_3 is the integral coefficient, K_{s2} is the sampling coefficient of the load-stage voltage sensor, and the reference voltage $v_{\mathrm{ref2}}(t)$ is $\sin(\omega t)$.

The triangular signal $v_{\mathrm{tri}}(t)$ is given in (5) shown at the bottom of this page, where T_{s2} is a switching period and V_{m2} is the amplitude of $v_{\mathrm{tri}}(t)$.

Suppose that the source-stage converter operates under continuous conduction mode, then the diode D and the switch S_0 will turn ON and OFF complementarily. In the load-stage inverter, one pair of switches S_1, S_4 and the other pair S_2, S_3 are also in complementary conduction.

B. Derivation of Nonlinear Averaged Equations

As is known well, a state averaged approach is used to characterize the dynamics of power switching converters [27]. Based

$$v_{\mathrm{tri}}(t) = \begin{cases} \dfrac{4V_{m2}}{T_{s2}}t - V_{m2} & nT_{s2} \le t < \left(n + \dfrac{1}{2}\right)T_{s2} \\ -\dfrac{4V_{m2}}{T_{s2}}t + 3V_{m2} & \left(n + \dfrac{1}{2}\right)T_{s2} < t \le (n+1)T_{s2} \end{cases} \quad (n = 0, 1, 2, \ldots) \tag{5}$$

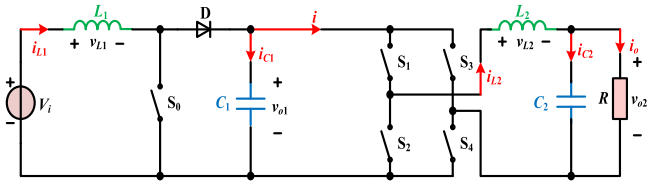

Fig. 2. Power stage of the two-stage boost inverter.

on the averaged approach, a set of nonlinear averaged equations will be derived for the two-stage boost inverter.

1) Power Stage: The power stage of the two-stage boost inverter is illustrated in Fig. 2. Here, we assume that i_{L1}, i_{L2}, i_{C1}, i_{C2}, i_o, v_{L1}, v_{L2}, v_{o1}, and v_{o2} represent the corresponding averaged variables within one switching period, respectively. Then, according to the power balance principle, the following expression can be obtained:

$$-V_i i_{L1} + v_{L1} i_{L1} + v_{o1} i_{C1} + v_{L2} i_{L2} + v_{o2} i_{C2} + v_{o2} i_o = 0. \tag{6}$$

Suppose that d_1 and d_2 are the duty cycles of the source stage and the load stage, then a set of differential equations with respect to L_1,C_1 and C_2 are given as

$$\begin{cases} L_1 \dfrac{\mathrm{d}i_{L1}}{\mathrm{d}t} = V_i - (1-d_1)v_{o1} \\ C_1 \dfrac{\mathrm{d}v_{o1}}{\mathrm{d}t} = (1-d_1)i_{L1} - (2d_2-1)i_{L2} \\ C_2 \dfrac{\mathrm{d}v_{o2}}{\mathrm{d}t} = i_{L2} - \dfrac{1}{R}v_{o2} \end{cases}. \tag{7}$$

Substituting (7) into (6), the power balance (6) can then be rewritten as

$$V_i i_{L1} = [V_i - (1-d_1)v_{o1}]\, i_{L1} + v_{o1}[(1-d_1)i_{L1} - (2d_2-1)i_{L2}] + L_2 \frac{\mathrm{d}i_{L2}}{\mathrm{d}t} i_{L2} + v_{o2}(i_{L2} - i_o) + v_{o2} i_o. \tag{8}$$

By simplifying (8), the following differential equation of i_{L2} can be obtained as:

$$L_2 \frac{\mathrm{d}i_{L2}}{\mathrm{d}t} = (2d_2 - 1)v_{o1} - v_{o2}. \tag{9}$$

By combining (7) and (9), the averaged equations of the power stage are derived as follows:

$$\begin{cases} L_1 \dfrac{\mathrm{d}i_{L1}}{\mathrm{d}t} = V_i - (1-d_1)v_{o1} \\ C_1 \dfrac{\mathrm{d}v_{o1}}{\mathrm{d}t} = (1-d_1)i_{L1} - (2d_2-1)i_{L2} \\ L_2 \dfrac{\mathrm{d}i_{L2}}{\mathrm{d}t} = (2d_2-1)v_{o1} - v_{o2} \\ C_2 \dfrac{\mathrm{d}v_{o2}}{\mathrm{d}t} = i_{L2} - \dfrac{1}{R}v_{o2} \end{cases}. \tag{10}$$

2) Control Circuit: The controller of the source-stage converter is composed of voltage outer loop and current inner loop. Based on (1) and (2), the differential equations of controller are given as

$$\frac{\mathrm{d}i_{\mathrm{ref1}}}{\mathrm{d}t} = -\frac{K_1 K_{s1}}{C_1}(1-d_1)i_{L1} + \frac{K_1 K_{s1}}{C_1}(2d_2-1)i_{L2} - \frac{K_1 K_{s1}}{T_1}v_{o1} + \frac{K_1}{T_1}V_{\mathrm{ref1}} \tag{11}$$

$$\frac{\mathrm{d}v_{\mathrm{con1}}}{\mathrm{d}t} = -\frac{K_2}{T_2}i_{L1} - \frac{K_1 K_2 K_{s1}}{C_1}(1-d_1)i_{L1} - \frac{K_1 K_2 K_{s1}}{T_1}v_{o1} + \frac{K_2}{T_2}i_{\mathrm{ref1}} + \frac{K_2}{L_1}(1-d_1)v_{o1} + \frac{K_1 K_2 K_{s1}}{C_1}(2d_2-1)i_{L2} + \frac{K_1 K_2}{T_1}V_{\mathrm{ref1}} - \frac{K_2}{L_1}V_i. \tag{12}$$

The PWM module can be described as [4]

$$d_1 = \frac{v_{\mathrm{con1}}}{V_{m1}}. \tag{13}$$

For the load-stage voltage controller, the following differential equation can be derived:

$$\frac{\mathrm{d}v_{\mathrm{con2}}}{\mathrm{d}t} = -\frac{K_3 K_{s2}}{C_2}i_{L2} + \left(\frac{K_3 K_{s2}}{RC_2} - \frac{K_3 K_{s2}}{T_3}\right)v_{o2} + \frac{K_3}{T_3}V_{\mathrm{ref2}}\sin(\omega t) + K_3 V_{\mathrm{ref2}}\omega\cos(\omega t). \tag{14}$$

Additionally, the SPWM module of the load-stage control circuit can be described as follows [27]:

$$d_2 = \frac{1}{2}\left(1 + \frac{v_{\mathrm{con2}}}{V_{m2}}\right). \tag{15}$$

Here, let $d = 2d_2 - 1$, then (15) can be rewritten as

$$d = 2d_2 - 1 = \frac{v_{\mathrm{con2}}}{V_{m2}}. \tag{16}$$

Combining (10)–(14) and (16), the two-stage boost inverter can be described by the following nonlinear averaged equations:

$$\begin{cases} \dfrac{\mathrm{d}i_{L1}}{\mathrm{d}t} = -\dfrac{1}{L_1}v_{o1} + \dfrac{1}{L_1}d_1 v_{o1} + \dfrac{1}{L_1}V_i \\ \dfrac{\mathrm{d}v_{o1}}{\mathrm{d}t} = \dfrac{1}{C_1}i_{L1} - \dfrac{1}{C_1}d_1 i_{L1} - \dfrac{1}{C_1}d i_{L2} \\ \dfrac{\mathrm{d}i_{\mathrm{ref1}}}{\mathrm{d}t} = -\dfrac{K_1 K_{s1}}{C_1}i_{L1} - \dfrac{K_1 K_{s1}}{T_1}v_{o1} + \dfrac{K_1 K_{s1}}{C_1}d_1 i_{L1} + \dfrac{K_1 K_{s1}}{C_1}d i_{L2} + \dfrac{K_1}{T_1}V_{\mathrm{ref1}} \\ \dfrac{\mathrm{d}d_1}{\mathrm{d}t} = \alpha_1 i_{L1} + \alpha_2 v_{o1} + \alpha_3 i_{\mathrm{ref1}} + \alpha_4 d_1 i_{L1} + \alpha_5 d_1 v_{o1} + \alpha_6 d i_{L2} + \alpha_7 V_{\mathrm{ref1}} + \alpha_8 V_i \\ \dfrac{\mathrm{d}i_{L2}}{\mathrm{d}t} = -\dfrac{1}{L_2}v_{o2} + \dfrac{1}{L_2}d v_{o1} \\ \dfrac{\mathrm{d}v_{o2}}{\mathrm{d}t} = \dfrac{1}{C_2}i_{L2} - \dfrac{1}{RC_2}v_{o2} \\ \dfrac{\mathrm{d}d}{\mathrm{d}t} = \beta_1 i_{L2} + \beta_2 v_{o2} + \beta_3\sin(\omega t) + \beta_4\cos(\omega t) \end{cases} \tag{17}$$

where

$$\alpha_1 = -\frac{1}{V_{m1}}\left(\frac{K_2}{T_2} + \frac{K_1K_2K_{s1}}{C_1}\right),$$
$$\alpha_2 = \frac{1}{V_{m1}}\left(\frac{K_2}{L_1} - \frac{K_1K_2K_{s1}}{T_1}\right),\ \alpha_3 = \frac{K_2}{V_{m1}T_2},$$
$$\alpha_4 = \frac{K_1K_2K_{s1}}{C_1V_{m1}},\ \alpha_5 = -\frac{K_2}{V_{m1}L_1},\ \alpha_6 = \frac{K_1K_2K_{\bar{s}1}}{V_{m1}C_1},$$
$$\alpha_7 = \frac{K_1K_2}{V_{m1}T_1},\ \alpha_8 = -\frac{K_2}{V_{m1}L_1},\ \beta_1 = -\frac{K_3K_{s2}}{V_{m2}C_2}$$
$$\beta_2 = \frac{1}{V_{m2}}\left(\frac{K_3K_{s2}}{RC_2} - \frac{K_3K_{s2}}{T_3}\right),\ \beta_3 = \frac{K_3V_{\mathrm{ref}2}}{V_{m2}T_3},$$

and

$$\beta_4 = \frac{K_3}{V_{m2}}V_{\mathrm{ref}2}\omega.$$

From (17), it is clear that the nonlinear averaged equations of the two-stage boost inverter are time-variant, and further are divided into the two parts: the first to forth equations are used to describe the dynamics of dc state variables (signals) with the hidden second-harmonic frequency[1] in the source stage and the fifth to seventh equations do the dynamics of ac state variables (signals) with the fundamental frequency in the load stage.

III. Observer-Pattern Modeling

It is known that appropriate modeling has a decisive influence on simplifying the analysis of dynamical systems. Actually, the nonlinear averaged equations (17) are time variant, which can lead to a great deal of trouble in system modeling and analysis. Therefore, how to eliminate the effect of time-variance is very helpful in not only uncovering the underlying mechanism of complex behaviors, but also providing more design-oriented information. To achieve the above goal, an observer-pattern model will be proposed, as follows.

1) Eliminating the time variance from the fundamental component in the load stage: Reconstructing each imaginary orthogonal variable corresponding to each physical state variable, and then performing the Park orthogonal transformation locally.
2) Eliminating the time variance from the hidden second-harmonic component in the source stage: Unmasking the hidden second harmonics in terms of the instantaneous power balance principle, and then performing the autonomous transformation locally.

Here, the nomenclature in the observer-pattern model is listed in Table I so as to make the derivation more understandable.

[1]As mentioned in [24]–[26], the second-harmonic component is always observed in the time-domain waveforms of all state variables in the source stage. Strangely, this harmonic component cannot be found out intuitively except calculating the nonlinear equations of the source stage. That is, this harmonic component seems to be hidden in the first to forth equations of (17).

TABLE I
Nomenclature in the Observer-Pattern Model

Symbol	Signification
i_{L2}, v_{o2}, d	Physical state variable in the load stage
i_{L2i}, v_{o2i}, d_i	Imaginary orthogonal variables in the load stage
$\boldsymbol{T}$	Park transformation matrix
i_{L2d}, v_{o2d}, d_d	Direct-axis component of state variables in the load stage
i_{L2q}, v_{o2q}, d_q	Quadrature-axis component of state variables in the load stage
g, g_1, g_2	Autonomous state variables with hidden second-harmonic component in the source stage

A. Eliminate the Time Variance From the Fundamental Component in the Load Stage

Since all three physical state variables i_{L2}, v_{o2}, and d are sinusoidal, the corresponding imaginary orthogonal variables i_{L2i}, v_{o2i}, and d_i can be reconstructed if the three physical variables are delayed for 90^{o}. Obviously, the acquired three pairs of the orthogonal variables should satisfy the following expressions:

$$\begin{cases} \dfrac{\mathrm{d}}{\mathrm{d}t}\begin{bmatrix} i_{L2} \\ i_{L2i} \end{bmatrix} = -\dfrac{1}{L_2}\begin{bmatrix} v_{o2} \\ v_{o2i} \end{bmatrix} + \dfrac{v_{o1}}{L_2}\begin{bmatrix} d \\ d_i \end{bmatrix} \\ \dfrac{\mathrm{d}}{\mathrm{d}t}\begin{bmatrix} v_{o2} \\ v_{o2i} \end{bmatrix} = \dfrac{1}{C_2}\begin{bmatrix} i_{L2} \\ i_{L2\mathrm{i}} \end{bmatrix} - \dfrac{1}{RC_2}\begin{bmatrix} v_{o2} \\ v_{o2i} \end{bmatrix} \\ \dfrac{\mathrm{d}}{\mathrm{d}t}\begin{bmatrix} d \\ d_i \end{bmatrix} = \beta_1\begin{bmatrix} i_{L2} \\ i_{L2i} \end{bmatrix} + \beta_2\begin{bmatrix} v_{o2} \\ v_{o2\vec{i}} \end{bmatrix} + \beta_3\begin{bmatrix} \sin(\omega t) \\ -\cos(\omega t) \end{bmatrix} \\ \qquad\qquad +\beta_4\begin{bmatrix} \cos(\omega t) \\ \sin(\omega t) \end{bmatrix} \end{cases}. \tag{18}$$

Performing the Park orthogonal transformation on the three pairs of the orthogonal variables [28], [29], we can obtain

$$\begin{cases} \dfrac{\mathrm{d}}{\mathrm{d}t}\left(\boldsymbol{T}^{-1}\begin{bmatrix} i_{L2d} \\ i_{L2q} \end{bmatrix}\right) = -\dfrac{1}{L_2}\boldsymbol{T}^{-1}\begin{bmatrix} v_{o2d} \\ v_{o2q} \end{bmatrix} + \dfrac{v_{o1}}{L_2}\boldsymbol{T}^{-1}\begin{bmatrix} d_d \\ d_q \end{bmatrix} \\ \dfrac{\mathrm{d}}{\mathrm{d}t}\left(\boldsymbol{T}^{-1}\begin{bmatrix} v_{o2d} \\ v_{o2q} \end{bmatrix}\right) = \dfrac{1}{C_2}\boldsymbol{T}^{-1}\begin{bmatrix} i_{L2d} \\ i_{L2q} \end{bmatrix} - \dfrac{1}{RC_2}\boldsymbol{T}^{-1}\begin{bmatrix} v_{o2d} \\ v_{o2q} \end{bmatrix} \\ \dfrac{\mathrm{d}}{\mathrm{d}t}\left(\boldsymbol{T}^{-1}\begin{bmatrix} d_d \\ d_q \end{bmatrix}\right) = \beta_1\boldsymbol{T}^{-1}\begin{bmatrix} i_{L2d} \\ i_{L2q} \end{bmatrix} + \beta_2\boldsymbol{T}^{-1}\begin{bmatrix} v_{o2d} \\ v_{o2q} \end{bmatrix} \\ \qquad\qquad +\boldsymbol{T}^{-1}\beta_3\begin{bmatrix} \sin(\omega t) \\ -\cos(\omega t) \end{bmatrix} \\ \qquad\qquad +\boldsymbol{T}^{-1}\beta_4\begin{bmatrix} \cos(\omega t) \\ \sin(\omega t) \end{bmatrix} \end{cases} \tag{19}$$

where

$$\boldsymbol{T}=\begin{bmatrix}\cos\omega t & \sin\omega t\\ -\sin\omega t & \cos\omega t\end{bmatrix}.$$

Since

$$\boldsymbol{T}\frac{\mathrm{d}\boldsymbol{T}^{-1}}{\mathrm{d}t}=\begin{bmatrix}\cos\omega t & \sin\omega t\\ -\sin\omega t & \cos\omega t\end{bmatrix}\begin{bmatrix}-\omega\sin\omega t & -\omega\cos\omega t\\ \omega\cos\omega t & -\omega\sin\omega t\end{bmatrix}=\begin{bmatrix}0 & -\omega\\ \omega & 0\end{bmatrix},$$

the equivalent model of the load-stage inverter (19) can be rewritten as

$$\begin{cases}\dfrac{\mathrm{d}}{\mathrm{d}t}\begin{bmatrix}i_{L2d}\\ i_{L2q}\end{bmatrix}=\begin{bmatrix}0 & \omega\\ -\omega & 0\end{bmatrix}\begin{bmatrix}i_{L2d}\\ i_{L2q}\end{bmatrix}-\dfrac{1}{L_2}\begin{bmatrix}v_{o2d}\\ v_{o2q}\end{bmatrix}+\dfrac{v_{o1}}{L_2}\begin{bmatrix}d_d\\ d_q\end{bmatrix}\\ \dfrac{\mathrm{d}}{\mathrm{d}t}\begin{bmatrix}v_{o2d}\\ v_{o2q}\end{bmatrix}=\dfrac{1}{C_2}\begin{bmatrix}i_{L2d}\\ i_{L2q}\end{bmatrix}+\begin{bmatrix}0 & \omega\\ -\omega & 0\end{bmatrix}\begin{bmatrix}v_{o2d}\\ v_{o2q}\end{bmatrix}-\dfrac{1}{RC_2}\begin{bmatrix}v_{o2d}\\ v_{o2q}\end{bmatrix}\\ \dfrac{\mathrm{d}}{\mathrm{d}t}\begin{bmatrix}d_d\\ d_q\end{bmatrix}=\beta_1\begin{bmatrix}i_{L2d}\\ i_{L2q}\end{bmatrix}+\beta_2\begin{bmatrix}v_{o2d}\\ v_{o2q}\end{bmatrix}+\begin{bmatrix}0 & \omega\\ -\omega & 0\end{bmatrix}\begin{bmatrix}d_d\\ d_q\end{bmatrix}\\ \qquad\qquad+\beta_3\begin{bmatrix}0\\ -1\end{bmatrix}+\beta_4\begin{bmatrix}1\\ 0\end{bmatrix}\end{cases}\tag{20}$$

where (i_{L2d}, i_{L2q}) (v_{o2d}, v_{o2q}), and (d_d, d_q) are the three pairs of the orthogonal variables (i_{L2}, i_{L2i}),(v_{o2}, v_{o2i}), and (d, d_i) in terms of the Park orthogonal transformation, respectively.

B. Eliminate the Time Variance From the Hidden Second-Harmonic Component in the Source Stage

In actual applications, the reactive power of the H-bridge inverter is negligible. Therefore, the input instantaneous active power of the load-stage inverter is $P(t)=\frac{1}{2}(v_d i_d+v_q i_q)[1-\cos(2\omega t)]$. According to the instantaneous power balance between the source stage and load stage, the nonlinear coupling effect between two subsystems can be unmasked by the following model of the source-stage converter:

$$\begin{cases}\dfrac{\mathrm{d}i_{L1}}{\mathrm{d}t}=-\dfrac{1}{L_1}v_{o1}+\dfrac{1}{L_1}d_1v_{o1}+\dfrac{1}{L_1}V_i\\ \dfrac{\mathrm{d}v_{o1}}{\mathrm{d}t}=\dfrac{1}{C_1}i_{L1}-\dfrac{1}{C_1}d_1i_{L1}-\dfrac{1}{2C_1}(d_di_{L2d}+d_qi_{L2q})\\ \qquad\times[1-\cos(2\omega t)]\\ \dfrac{\mathrm{d}i_{\mathrm{ref1}}}{\mathrm{d}t}=-\dfrac{K_1K_{s1}}{C_1}i_{L1}-\dfrac{K_1K_{s1}}{T_1}v_{o1}+\dfrac{K_1K_{s1}}{C_1}d_1i_{L1}\\ \qquad+\dfrac{K_1K_{s1}}{2C_1}(d_di_{L2d}+d_qi_{L2q})[1-\cos(2\omega t)]\\ \qquad+\dfrac{K_1}{T_1}V_{\mathrm{ref1}}\\ \dfrac{\mathrm{d}d_1}{\mathrm{d}t}=\alpha_1i_{L1}+\alpha_2v_{o1}+\alpha_3i_{\mathrm{ref1}}+\alpha_4d_1i_{L1}+\alpha_5d_1v_{o1}\\ \qquad+\dfrac{\alpha_6}{2}(d_di_{L2d}+d_qi_{L2q})[1-\cos(2\omega t)]\\ \qquad+\alpha_7V_{\mathrm{ref1}}+\alpha_8V_i\end{cases}\tag{21}$$

As can be seen in (21), the averaged equations contain a time-variant term $\cos(2\omega t)$, i.e., it is still a nonautonomous system. Since $\cos(2\omega t)$ is one solution of the differential equation $\ddot{g}+4\omega^2 g=0$, it yields the following equations:

$$\begin{cases}\dfrac{\mathrm{d}g_1}{\mathrm{d}t}=g_2\\ \dfrac{\mathrm{d}g_2}{\mathrm{d}t}=-4\omega^2g_1\end{cases}\tag{22}$$

where the initial conditions are $g_1(0)=1$ and $g_2(0)=0$.

Combining (20)–(22), the complete observer-pattern model of the two-stage boost inverter can then be described as

$$\begin{cases}\dfrac{\mathrm{d}i_{L1}}{\mathrm{d}t}=-\dfrac{1}{L_1}v_{o1}+\dfrac{1}{L_1}d_1v_{o1}+\dfrac{1}{L_1}V_i\\ \dfrac{\mathrm{d}v_{o1}}{\mathrm{d}t}=\dfrac{1}{C_1}i_{L1}-\dfrac{1}{C_1}d_1i_{L1}-\dfrac{1}{2C_1}(d_di_{L2d}+d_qi_{L2q})(1-g_1)\\ \dfrac{\mathrm{d}i_{\mathrm{ref1}}}{\mathrm{d}t}=-\dfrac{K_1K_{s1}}{C_1}i_{L1}-\dfrac{K_1K_{s1}}{T_1}v_{o1}+\dfrac{K_1K_{s1}}{C_1}d_1i_{L1}\\ \qquad+\dfrac{K_1K_{s1}}{2C_1}(d_di_{L2d}+d_qi_{L2q})(1-g_1)+\dfrac{K_1}{T_1}V_{\mathrm{ref1}}\\ \dfrac{\mathrm{d}d_1}{\mathrm{d}t}=\alpha_1i_{L1}+\alpha_2v_{o1}+\alpha_3i_{\mathrm{ref1}}+\alpha_4d_1i_{L1}+\alpha_5d_1v_{o1}\\ \qquad+\dfrac{\alpha_6}{2}(d_di_{L2d}+d_qi_{L2q})(1-g_1)+\alpha_7V_{\mathrm{ref1}}+\alpha_8V_i\\ \dfrac{\mathrm{d}i_{L2d}}{\mathrm{d}t}=\omega i_{L2q}-\dfrac{1}{L_2}v_{o2d}+\dfrac{1}{L_2}d_dv_{o1}\\ \dfrac{\mathrm{d}i_{L2q}}{\mathrm{d}t}=-\omega i_{L2d}-\dfrac{1}{L_2}v_{o2q}+\dfrac{1}{L_2}d_qv_{o1}\\ \dfrac{\mathrm{d}v_{o2d}}{\mathrm{d}t}=\dfrac{1}{C_2}i_{L2d}+\omega v_{o2q}-\dfrac{1}{RC_2}v_{o2d}\\ \dfrac{\mathrm{d}v_{o2q}}{\mathrm{d}t}=\dfrac{1}{C_2}i_{L2q}-\omega v_{o2d}-\dfrac{1}{RC_2}v_{o2q}\\ \dfrac{\mathrm{d}d_d}{\mathrm{d}t}=\beta_1i_{L2d}+\beta_2v_{o2d}+\omega d_q+\beta_4\\ \dfrac{\mathrm{d}d_q}{\mathrm{d}t}=\beta_1i_{L2q}+\beta_2v_{o2q}-\omega d_d-\beta_3\\ \dfrac{\mathrm{d}g_1}{\mathrm{d}t}=g_2\\ \dfrac{\mathrm{d}g_2}{\mathrm{d}t}=-4\omega^2g_1\end{cases}\tag{23}$$

For simplicity, let

$$\boldsymbol{X}=[i_{L1}, v_{o1}, i_{\mathrm{ref1}}, d_1, i_{L2d}, i_{L2q}, v_{o2d}, v_{o2q}, d_d, d_q, g_1, g_2]^{\mathrm{T}},$$

then (23) can be rewritten in the following compact form:

$$\dot{\boldsymbol{X}}=\boldsymbol{F}(\boldsymbol{X})\qquad(\boldsymbol{F}: R^{12}\to R^{12})\tag{24}$$

where each element of the smooth vector field $\boldsymbol{F}=[F_1, F_2, F_3, F_4, F_5, F_6, F_7, F_8, F_9, F_{10}, F_{11}, F_{12}]^T$ is

$$F_1 = -\frac{1}{L_1}v_{o1} + \frac{1}{L_1}d_1 v_{o1} + \frac{1}{L_1}V_i,$$

$$F_2 = \frac{1}{C_1}i_{L1} - \frac{1}{C_1}d_1 i_{L1} - \frac{1}{2C_1}(d_d i_{L2d} + d_q i_{L2q})(1-g_1),$$

$$F_3 = -\frac{K_1K_{s1}}{C_1}i_{L1} - \frac{K_1K_{s1}}{T_1}v_{o1} + \frac{K_1K_{s1}}{C_1}d_1 i_{L1} + \frac{K_1K_{s1}}{2C_1}(d_d i_{L2d} + d_q i_{L2q})(1-g_1) + \frac{K_1}{T_1}V_{\mathrm{ref}1},$$

$$F_4 = \alpha_1 i_{L1} + \alpha_2 v_{o1} + \alpha_3 i_{\mathrm{ref}1} + \alpha_4 d_1 i_{L1} + \alpha_5 d_1 v_{o1} + \frac{\alpha_6}{2}(d_d i_{L2d} + d_q i_{L2q})(1-g_1) + \alpha_7 V_{\mathrm{ref}1} + \alpha_8 V,$$

$$F_5 = \omega i_{L2q} - \frac{1}{L_2}v_{o2d} + \frac{1}{L_2}d_d v_{o1},$$

$$F_6 = -\omega i_{L2d} - \frac{1}{L_2}v_{o2q} + \frac{1}{L_2}d_q v_{o1},$$

$$F_7 = \frac{1}{C_2}i_{L2d} + \omega v_{o2q} - \frac{1}{RC_2}v_{o2d},$$

$$F_8 = \frac{1}{C_2}i_{L2q} - \omega v_{o2d} - \frac{1}{RC_2}v_{o2q},$$

$$F_9 = \beta_1 i_{L2d} + \beta_2 v_{o2d} + \omega d_q + \beta_4,$$

$$F_{10} = \beta_1 i_{L2q} + \beta_2 v_{o2q} - \omega d_d - \beta_3,$$

$$F_{11} = g_2$$

and

$$F_{12} = -4\omega^2 g_1,$$

respectively.

IV. Nonlinear Modal Representation

From (24), it is evident that the two-stage boost inverter inherently belongs to one class of strongly nonlinear coupling systems. In fact, nonlinear modal analysis method is found to be one powerful and effective tool, which can straightly access the high-frequency information and the underlying interaction characteristics of the transient behaviors [30]. Hence, this method will be used to derive the nonlinear modal representation of the two-stage boost inverter.

Suppose that the equilibrium point of the two-stage boost inverter is

$$\boldsymbol{X}_e = [i_{L1}^e, v_{o1}^e, i_{\mathrm{ref}1}^e, d_1^e, i_{L2d}^e, i_{L2q}^e, v_{o2d}^e, v_{o2q}^e, d_d^e, d_q^e, g_1^e, g_2^e]^T,$$

then we can take the Taylor expansion on (24) at $\boldsymbol{X}_e$ and yield the following perturbed expression [27]:

$$\dot{\boldsymbol{X}} = \boldsymbol{A}\boldsymbol{X} + \frac{1}{2}\begin{bmatrix} \boldsymbol{X}^T\boldsymbol{H}_1\boldsymbol{X} \\ \boldsymbol{X}^T\boldsymbol{H}_2\boldsymbol{X} \\ \vdots \\ \boldsymbol{X}^T\boldsymbol{H}_{12}\boldsymbol{X} \end{bmatrix} + \cdots \tag{25}$$

where $\boldsymbol{X}$ belongs to the convergence domain of the Taylor series, $\boldsymbol{A} = [\partial F_i/\partial \boldsymbol{X}]_{\boldsymbol{X}=\boldsymbol{X}_e}$ is the Jacobian matrix given in Appendix A, and $\boldsymbol{H}_i = [\partial^2 F_i/\partial x_k \partial x_l]_{\boldsymbol{X}=\boldsymbol{X}_e}(i,k,l = 1,2,\ldots,12)$ is the Hessian Matrix given in Appendix B.

Assume that $\lambda_j (j = 1,2,\ldots,12)$ denotes 12 distinct eigenvalues of $\boldsymbol{A}$, and $\boldsymbol{\Lambda}$ denotes the Jordan form of $\boldsymbol{A}$, $\boldsymbol{U}$ represents the matrix of the right eigenvector, and $\boldsymbol{V}$ indicates the inverse matrix of $\boldsymbol{U}$, then by using $\boldsymbol{X} = \boldsymbol{U}\boldsymbol{Y}$, (25) can be rearranged as

$$\dot{\boldsymbol{Y}} = \boldsymbol{\Lambda}\boldsymbol{Y} + \frac{1}{2}\boldsymbol{V}^H \begin{bmatrix} \boldsymbol{Y}^T(\boldsymbol{U}^T\boldsymbol{H}_1\boldsymbol{U})\boldsymbol{Y} \\ \boldsymbol{Y}^T(\boldsymbol{U}^T\boldsymbol{H}_2\boldsymbol{U})\boldsymbol{Y} \\ \vdots \\ \boldsymbol{Y}^T(\boldsymbol{U}^T\boldsymbol{H}_{12}\boldsymbol{U})\boldsymbol{Y} \end{bmatrix} + \cdots. \tag{26}$$

Thus, (26) can be rewritten as

$$\dot{y}_j = \lambda_j y_j + \sum_{k=1}^{12}\sum_{l=1}^{12} C_{kl}^j y_k y_l + \cdots \tag{27}$$

where $\boldsymbol{C}^j = [C_{kl}^j] = \frac{1}{2}\sum_{p=1}^{12} v_{jp}[\boldsymbol{U}^T\boldsymbol{H}_p\boldsymbol{U}]$ and v_{jp} is the jth element of the pth column of $\boldsymbol{V}$, respectively.

Note that the solution of (27) can be decomposed into $y_j(t) = f_{1j}(t) + f_{2j}(t) + f_{3j}(t) + \cdots$, where $f_{mj}(t)$ contains the terms dependent on any m-states multiples of initial conditions. Thus, (27) can be rearranged as

$$\begin{cases} \dot{f}_{1j} = \lambda_j f_{1j} \\ \dot{f}_{2j} = \lambda_j f_{2j} + \sum_{k=1}^{12}\sum_{l=1}^{12} C_{kl}^j f_{1k} f_{1l} \\ \vdots \end{cases}. \tag{28}$$

If both the first term and second term in Taylor expansion series are reserved [28], then the nonlinear modal analytical solution can be obtained by the inverse Laplace transform

$$\begin{aligned} y_j(t) = y_{1j}(t) + y_{2j}(t) &= y_{j0}e^{\lambda_j t} + \sum_{k=1}^{12}\sum_{l=1}^{12} C_{kl}^j S_{kl}^j(t) \\ &= \left(y_{j0} - \sum_{k=1}^{12}\sum_{l=1}^{12} h2_{kl}^j y_{k0} y_{l0}\right)e^{\lambda_j t} \\ &\quad + \sum_{k=1}^{12}\sum_{l=1}^{12} h2_{kl}^j y_{k0} y_{l0} e^{(\lambda_k+\lambda_l)t} \end{aligned} \tag{29}$$

where $k,l,j = 1,2,\ldots,12$ and $h2_{kl}^j = C_{kl}^j/(\lambda_k + \lambda_l - \lambda_j)$.

Finally, the nonlinear modal representation of the system can be expressed as

$$x_i(t) = \sum_{j=1}^{12} L_j^i e^{\lambda_j t} + \sum_{k=1}^{12}\sum_{l=1}^{12} K_{kl}^i e^{(\lambda_k+\lambda_l)t} \tag{30}$$

where $L_j^i = u_{ij}(y_{j0} - \sum_{k=1}^{12}\sum_{l=1}^{12} h2_{kl}^j y_{k0} y_{l0})$, and $K_{kl}^i = y_{k0}y_{l0}\sum_{j\in J_{kl}}^{12} u_{ij} h2_{kl}^j$, respectively.

From (30), the nonlinear modal representation of (24) contains the two terms, i.e., fundamental modal terms $\sum_{j=1}^{12} L_j^i e^{\lambda_j t}$ and second-order interacted modal terms $\sum_{k=1}^{12}\sum_{l=1}^{12} K_{kl}^i e^{(\lambda_k+\lambda_l)t}$. Note that the fundamental modal terms only indicate the influence of all fundamental modes on the system dynamical response, while the second-order interacted

TABLE II
COMPONENT PARAMETERS AND VALUES USED IN SIMULATION

Components/parameters	Values
Input voltage V_i	10 V
Inductance of the source and load subsystem L_1, L_2	1 mH, 1 mH
Capacitance of the source and load subsystem C_1, C_2	470 μF, 47 μF
Gain of voltage sensor K_{s1}, K_{s2}	0.1, 0.05
Proportional and integral coefficients of the source-stage voltage controller K_1, T_1	0.5, 0.001
Proportional and integral coefficients of the source-stage current controller K_2, T_2	0.5, 0.02
Proportional and integral coefficients of the load-stage voltage controller K_3, T_3	1.2, 0.0013
Source-stage reference voltage V_{ref1}	3 V
Load-stage reference voltage V_{ref2}	sin (100πt)V
Amplitude of sawtooth and triangular waves V_{m1}, V_{m2}	5 V, 1.5 V
Switching frequencies of the source stage and load stage f_{s1}, f_{s2}	20 kHz, 20 kHz

modal terms heavily do the influence of all second-order interacted modes. Comparing (30) with the linearized approach, we can see that nonlinear modal representation not only gives two explicit correction terms for initial values L_j^i and K_{kl}^i, but also provides an access to evaluate the nonlinear extent of the dynamical system. Thus, the nonlinear modal obtained here is sufficient to investigate the transient behavior of the two-stage boost inverter.

V. NONLINEAR MODAL ANALYSIS

A. Transient Phenomenon

Inevitably, the two-stage boost inverter suffers from a great variety of disturbances such as sudden load jump. During these transient process, the system may subject to overvoltage, overcurrent, and transient chaos, etc. This leads to the increase of device stress, the degradation of efficiency and reliability, or even the collapse of the system. In what follows, the load disturbance is taken as one example to investigate the nonlinear interactions in the transient process. The simulation parameters used here are given in Table II.

At the moment of $t = 0.6075$ s, with the sudden jump of R from 15 to 5Ω, the system will eventually reach one new stable state. Time-domain waveforms obtained by using the exact switch model and the nonlinear modal representation are shown in Fig. 3. Clearly, it can be seen from Fig. 3 that the waveforms obtained by using the nonlinear modal representation are closed to ones, by using the exact switch model both in stable behaviors and in transient ones, which verifies the validity of the nonlinear modal representation. Therefore, by taking into account high-frequency information of nonlinear interactions, nonlinear modal representation provides a good representation for the dynamics of the system both in the source stage and in the load stage.

For the sake of the comparison between nonlinear modal analysis approach and linearized analysis one, the modal distribution is depicted in Fig. 4. Note that as long as some mode appears in linearized or nonlinear modal analysis approach, the symbol of this mode will be filled with the pink color. By comparing

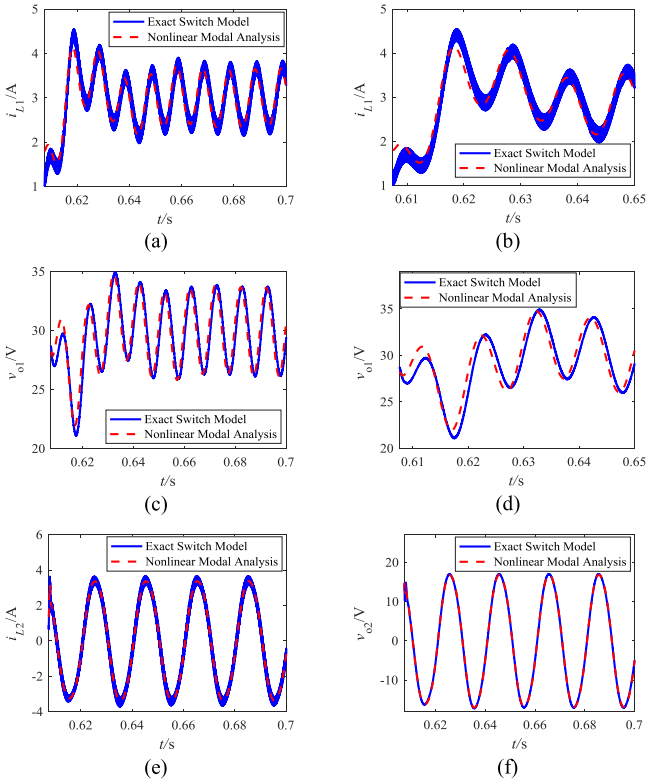

Fig. 3. Time-domain waveforms of the two-stage boost inverter from exact switch model and nonlinear modal analysis. (a) i_{L1}. (b) Close-up of i_{L1}. (c) v_{o1}. (d) Close-up of v_{o1}. (e) i_{L2}. (f) v_{o2}.

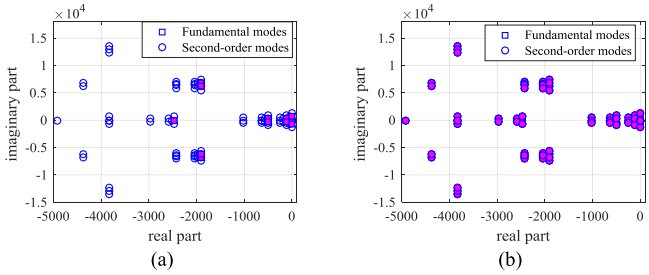

Fig. 4. Modal distribution: (a) Linearized analysis approach. (b) Nonlinear modal analysis approach.

Fig. 4(a) and (b), we can draw the conclusion that the linearized analysis approach is only involved with all fundamental modes, whereas the nonlinear modal analysis approach does all second-order interacted modes besides all fundamental ones. This just explains the reason why nonlinear modal analysis approach can be used to characterize the substantial high-frequency dynamics of the transient process.

B. Nonlinear Modal Analysis

As mentioned above, the nonlinear modal representation (30) can adequately describe the high-frequency dynamical information, which just plays a more important role in the transient behavior. Thus, the nonlinear modal analysis approach finds out a theoretical way to understand the system transient behavior from two points of view, i.e., both fundamental modal analysis and second-order interacted modal analysis, as follows.

TABLE III
FUNDAMENTAL MODES OF TWO-STAGE BOOST INVERTER DURING THE TRANSIENT PROCESS

Fundamental modes	values	Frequency /Hz	Damping ratio
$\lambda_{1,2}$	-1912.4 ± 6771.5i	1077.7	0.2718
$\lambda_{3,4}$	-1911.8 ± 6114.1i	973.09	0.2984
λ_5	-2737.6	–	–
$\lambda_{6,7}$	-461.25 ± 292.56i	46.562	0.8444
$\lambda_{8,9}$	-55.929 ± 171.04i	27.222	0.3108
λ_{10}	-57.366	–	–
$\lambda_{11,12}$	± 628.32i	100	0

1) Fundamental Modal Analysis: In order to obtain the primitive knowledge of the system behavior, all 12 fundamental modes are calculated through the Jacobian matrix A, as shown in Table III. Obviously, the real parts of ten fundamental modes are negative, which means that the system is still stable after the load disturbance. The four pairs of conjugate complex fundamental modes ($\lambda_{1,2}$, $\lambda_{3,4}$, $\lambda_{6,7}$, $\lambda_{8,9}$) belong to the oscillation modes, while the two negative real fundamental modes (λ_5, λ_{10}) do damping modes. Among all the ten fundamental modes, ($\lambda_{6,7}$, $\lambda_{8,9}$) are much closer to the imaginary axis, which implies that ($\lambda_{6,7}$, $\lambda_{8,9}$) are surely the dominant fundamental modes of this system. Note that there is one pair of conjugate imaginary modes $\lambda_{11,12}$, which is originated from the above differential equation $\ddot{g} + 4\omega^2 g = 0$. That is, $\lambda_{11,12}$ is independent of physical circuit parameters for the sake of the hidden second-harmonic component. Accordingly, we can neglect $\lambda_{11,12}$ and only take the other modes into consideration during the fundamental modal analysis.

Indeed, these fundamental modes play the direct role in the system transient behaviors as well as stable ones. In actual applications, some electrical engineers are concerned with identifying the correlation between system parameters and transient response. This is because such design-oriented information is quite useful to optimize the transient performance. From the fundamental modal terms in (30), it can be seen that the performance of transient response is determined by two parts, i.e., the initial value L_j^i and the contraction rate defined by the fundamental modes λ_j. Therefore, the transient response will be readily optimized if the correlation between the circuit system and the two parts is established.

a) Correlation between fundamental modes and state variables: To describe the correlation between the *j*th fundamental mode λ_j and the *i*th state variable x_i, nonlinear contribution factor c_{ij} will be defined to measure the contribution of the jth fundamental modes λ_j on the ith state variables x_i [12]

$$c_{ij} = \left| u_{ij} - \sum_{k=1}^{12} \sum_{l=1}^{12} u_{ij} h 2_{kl}^{j} \right|. \tag{31}$$

For simplicity, the three-dimensional (3-D) bar graph of the normalized nonlinear contribution factor is shown in Fig. 5. For $\lambda_{1,2}$ and $\lambda_{3,4}$, i_{L2}, v_{o2}, and d have larger contribution factor than other state variables. This implies that $\lambda_{1,2}$ and $\lambda_{3,4}$ are mostly associated with i_{L2}, v_{o2}, and d. Likewise, λ_5 is mainly associated with i_{L1} and d_1, whereas λ_{10} does on i_{ref}. In addition, the pair of the fundamental modes $\lambda_{6,7}$ has slight effect on all state variables. Surprisingly, although v_{o1} and i_{L1} are tightly related with $\lambda_{8,9}$, v_{o1} is more vulnerable to the effect of the dominant fundamental modes than i_{L1}. Note that the contribution factors of g_1 and g_2 with regard to $\lambda_1 \ldots \lambda_{10}$ are all zero. It means that g_1 and g_2 merely rely on $\lambda_{11,12}$ rather than others. This is just in agreement with the above analytical results.

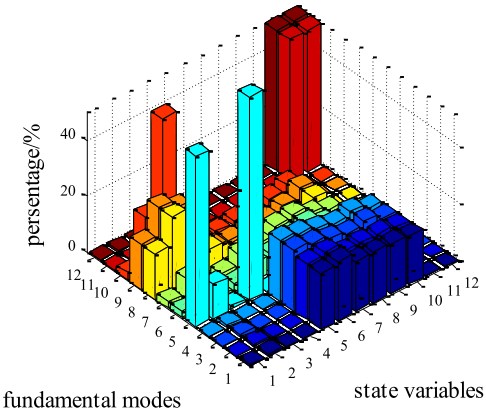

Fig. 5. Normalized nonlinear contribution factors c_{ij} of two-stage boost inverter.

b) Influence of circuit parameters on fundamental modes: Fundamental modal sensitivity analysis is an effective method to assess the impact of system parameters on the fundamental modes. The expression of the fundamental mode sensitivity is as follows:

$$S_{\alpha}^{\lambda_i} = \frac{\alpha_0}{\text{Re}(\lambda_i)} \frac{\partial \text{Re}(\lambda_i)}{\partial \alpha}\bigg|_{\alpha_0} + \text{i}\frac{\alpha_0}{\text{Im}(\lambda_i)} \frac{\partial \text{Im}(\lambda_i)}{\partial \alpha}\bigg|_{\alpha_0} \tag{32}$$

where α_0 is some given circuit parameter. Note that the fundamental mode sensitivity is intrinsically the normalized gradient of each fundamental mode with respect to one circuit parameter under study.

The fundamental mode sensitivities with respect to 11 circuit parameters are listed in Table IV. It can be seen that $\lambda_{1,2}$ and $\lambda_{3,4}$ are more sensitive to the two parameters C_2 and R than others. Moreover, the increase in C_2 or R will make $\lambda_{1,2}$ and $\lambda_{3,4}$ move toward the imaginary axis so that the system stability margin becomes smaller. λ_5 is sensitive to the five parameters L_1, L_2, K_1, T_1, and K_2. Different from $\lambda_{1,2}$ and $\lambda_{3,4}$, $\lambda_{6,7}$ shows extreme sensitivity to the two parameters K_3 and T_3. If K_3 decreases or T_3 increases, $\lambda_{6,7}$ will move toward left in the complex plane. This implies that the system stability margin becomes larger. Additionally, $\lambda_{8,9}$ is only sensitive to the power-stage parameter C_1. Therefore, we can find the key parameters of the two-stage boost inverter, i.e., power-stage parameters C_1 and control circuit parameters K_3 and T_3, which have notable influence on the dominant oscillation modes.

From the above two indices, i.e., nonlinear contribution factors and fundamental mode sensitivities, it can be concluded that $\lambda_{1,2}$ and $\lambda_{3,4}$ are tightly correlated with the load-stage subsystem, and $\lambda_{8,9}$ play the decisive role in the source-stage

TABLE IV
FUNDAMENTAL MODE SENSITIVITIES WITH RESPECT TO SYSTEM PARAMETERS

	$S^{\lambda 1,2}$	$S^{\lambda 3,4}$	$S^{\lambda 5}$	$S^{\lambda 6,7}$	$S^{\lambda 8,9}$	$S^{\lambda 10}$
L_1	$0.0040 \mp 0.4930i$	$0.0041 \mp 0.5409i$	1.0799	$-0.0173 \mp 0.0093i$	$-0.0253 \mp 0.5967i$	-0.1675
C_1	$0.0021 \mp 0.0019i$	$0.0015 \mp 0.0023i$	–0.0591	$0.0307 \pm 0.0414i$	$1.0695 \mp 0.4576i$	0.0127
L_2	$0.0046 \mp 0.487i$	$0.0039 \mp 0.5411i$	1.0642	$-0.0183 \mp 0.0091i$	$-0.0254 \mp 0.5963i$	-0.1596
C_2	$1.2457 \mp 0.4627i$	$1.2464 \mp 0.5074i$	–0.0004	$0.0090 \pm 0.0010i$	$0.0041 \mp 0.0008i$	0.0000
R	$1.2438 \pm 0.0283i$	$1.2440 \pm 0.0312i$	–0.0185	$0.0514 \pm 0.0351i$	$0.0438 \pm 0.0072i$	0.0024
K_1	$-0.0000 \pm 0.000i$	$-0.0000 \pm 0.000i$	–1.0877	$0.0015 \pm 0.0164i$	$0.4474 \pm 0.7154i$	0.3213
T_1	$0.0043 \mp 0.4821i$	$0.0045 \mp 0.5412i$	1.0621	$-0.0179 \mp 0.0087i$	$-0.0251 \mp 0.5963i$	-0.1657
K_2	$-0.0000 \mp 0.000i$	$-0.0000 \pm 0.000i$	–1.0877	$0.0015 \pm 0.0164i$	$0.4474 \pm 0.7154i$	0.3212
T_2	$-0.0000 \pm 0.000i$	$-0.0000 \pm 0.000i$	–0.0201	$-0.0002 \pm 0.0013i$	$-0.0911 \pm 0.0634i$	1.1529
K_3	$0.1069 \pm 0.2676i$	$0.1070 \pm 0.2938i$	0.0055	$-0.4397 \pm 0.0147i$	$0.0087 \pm 0.0042i$	0.0023
T_3	$-0.2511 \pm 0.001i$	$-0.2514 \pm 0.001i$	–0.0076	$1.0103 \pm 0.0005i$	$-0.1152 \pm 0.0124i$	-0.0029

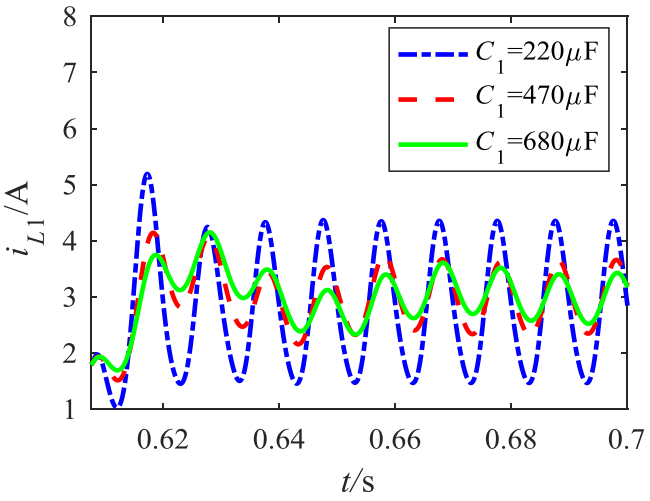

Fig. 6. Transient waveforms of inductor current i_{L1} under three different values of C_1.

subsystem. Decreasing the key parameters C_1 and T_3 will be beneficial to the dynamical response of each subsystem.

To verify the above conclusion of fundamental mode analysis, the comparison of the transient waveforms of inductor current i_{L1} under three different values of C_1 is given in Fig. 6. When C_1 decreases from 680 to 220 μF, the pair of the oscillation modes $\lambda_{8,9}$ strongly correlated with C_1 changes from $-37.8 \pm 144i$ to $-121.3 \pm 237i$. At the same time, the settling time decreases from 0.08 to 0.02 s. This implies that the system transient performance will do benefit from the proper choice of such key circuit parameters as C_1.

2) Second-Order Nonlinear Interacted Modal Analysis: In fact, there is one of the most distinguishing differences between nonlinear systems and linear ones, i.e., the natural nonlinearity is bound to activate a great varieties of higher order interacted modes besides those original fundamental ones [28]. Of course, these higher order nonlinear interacted modes (especially second-order interacted modes) generally contribute plenty of nonlinear dynamical features to transient behaviors and even stable ones.

For the purpose of evaluating the extent of nonlinear interactions, second-order nonlinear interaction indices $I2^i_{kl}$ will be defined according to the form of the second-order interacted modal terms in nonlinear modal representation [31]

$$I2^i_{kl} = \left| \frac{K^i_{kl}}{\mathrm{Re}(\lambda_k + \lambda_l)} \right| \qquad i = 1, 2, \ldots, 12. \tag{33}$$

In (33), K^i_{kl} represents the initial amplitude of second-order modes and $\mathrm{Re}(\lambda_k + \lambda_l)$ determines the attenuation rate. That is, the indices $I2^i_{kl}$ can comprehensively consider the amplitude and duration of interacted modes so that these indices are able to measure the influence of nonlinear transient interactions.

Theoretically, 12 fundamental modes can give rise to 144 second-order interacted modes in the two-stage boost inverter. For example, $\lambda_{k=1,l=3}$ represents the interaction between λ_1 and λ_3, i.e., mutual-action, whereas $\lambda_{k=3,l=3}$ does the interaction between λ_3 and itself, i.e., self-action. The 3-D bar graph of the index $I2^i_{kl}$ are plotted in Figs. 7 and 8. From Fig. 7, we can see that the two self-action $\lambda_{k=8,l=8}$ and $\lambda_{k=9,l=9}$ are the dominant interacted modes of the source-stage inductor current i_{L1}, while $\lambda_{k=8,9,l=8,9}$ are the guiding interacted modes of the source-stage capacitor voltage v_{o1}, active power component of the load-stage inductor current i_{L2d}, and active power component of the load-stage capacitor voltage v_{o2d}. For reactive power component of the load-stage inductor current i_{L2q} and reactive power component of the load-stage capacitor voltage v_{o2q}, $\lambda_{k=1,2,3,4,l=8,9}$ and $\lambda_{k=8,9,l=1,2,3,4}$ are also the dominant interacted modes besides $\lambda_{k=8,9,l=8,9}$.

When the control parameter K_1 decreases from 0.5 to 0.25, the dominant interactions of such state variables as i_{L1}, v_{o1}, and v_{o2d} have great variation. By comparing Figs. 7 with 8, it can be seen that both the dominant interacted modes and the magnitude of interaction index have altered with the variation of the control parameter K_1. Specifically, when $K_1 = 0.25$, $\lambda_{k=8,9,l=8,9}$ are the leading interacted modes in i_{L1}, whose interacted modes increase comparing Fig. 8(a) with Fig. 7(a), whereas the interacted modes $\lambda_{k=8,l=8}$ and $\lambda_{k=9,l=9}$ decrease in v_{o1}. Comparing Fig. 8(e) with Fig. 7(e), the dominant interacted modes become $\lambda_{k=8,9,10,l=8,9,10}$.

Furthermore, the second-order nonlinear interaction indices $\Delta I2^i_{kl}$ change with the variation of L_1, C_1, K_1, and K_2, as is shown in Fig. 9. It can be observed that most of the interaction indexes $\Delta I2^i_{kl}$ increase monotonically, such as v_{o2d} and v_{o2q} in Fig. 9(a), whereas most of the interaction indexes like i_{L2d} and i_{L2q} decrease monotonically in Fig. 9(b). From Fig. 9(c) and

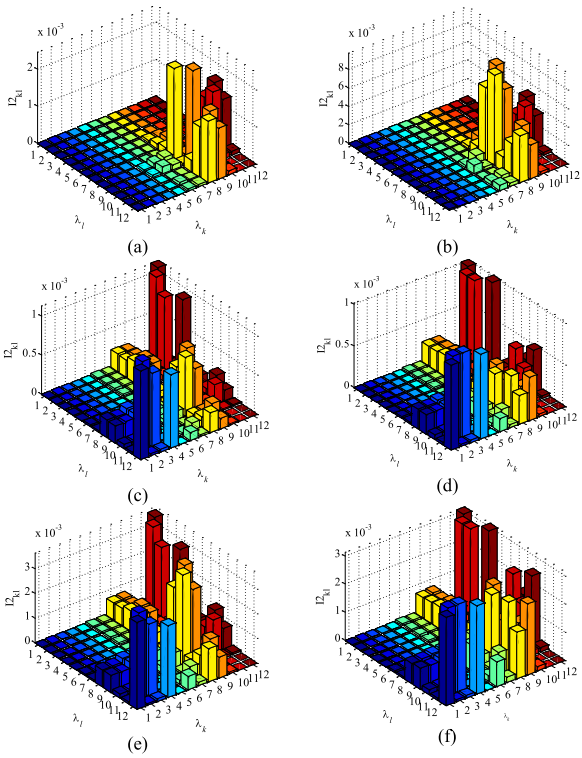

Fig. 7. Effects of modal interaction on the state variables of two-stage Boost inverter during the transient process when $K_1 = 0.5$, $K_2 = 0.5$. (a) Interaction of i_{L1}. (b) Interaction of v_{o1}. (c) Interaction of i_{L2d}. (d) Interaction of i_{L2q}. (e) Interaction of v_{o2d}. (f) Interaction of v_{o2q}.

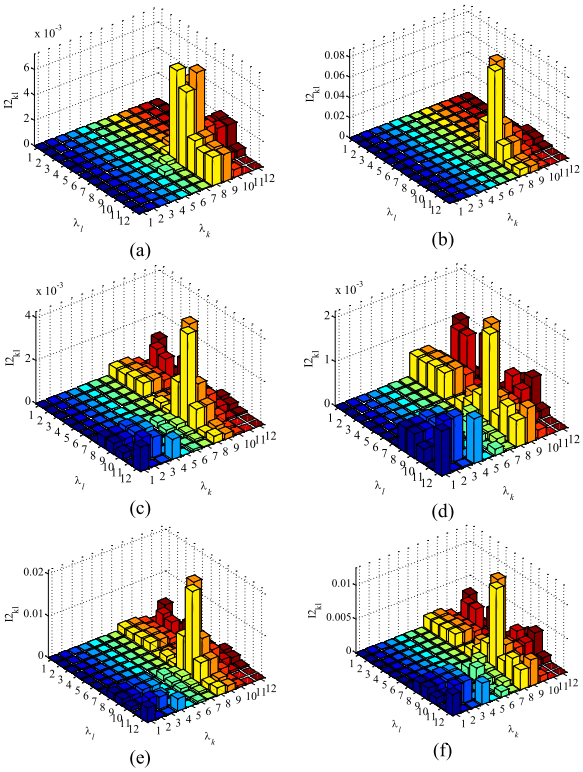

Fig. 8. Effects of modal interaction on the state variables of two-stage boost inverter during the transient process when $K_1 = 0.25$, $K_2 = 0.5$. (a) Interaction of i_{L1}. (b) Interaction of v_{o1} (c) Interaction of i_{L2d}. (d) Interaction of i_{L2q}. (e) Interaction of v_{o2d}. (f) Interaction of v_{o2q}.

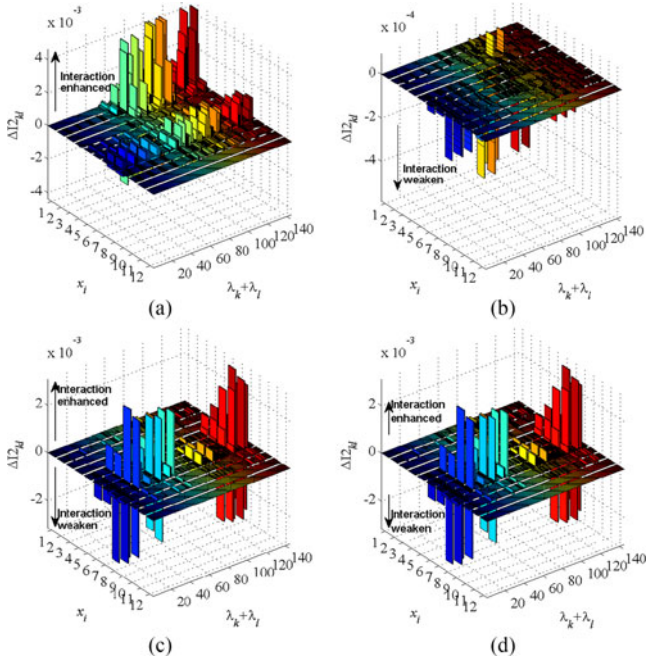

Fig. 9. Nonlinear interaction index variation during disturbed transient process when parameters vary. (a) L_1 increasing from 1 to 2.6 mH. (b) C_1 increasing from 380 to 620 μF. (c) K_1 increasing from 0.5 to 1.3. (d) K_2 increasing from 0.4 to 1.2.

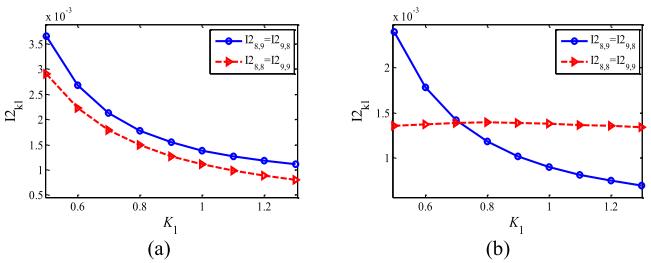

Fig. 10. Nonlinear interaction indices of dominant interacted modes when K_1 varies (a) dominant interacted modes of v_{o2d} (b) dominant interacted modes of v_{o2q}.

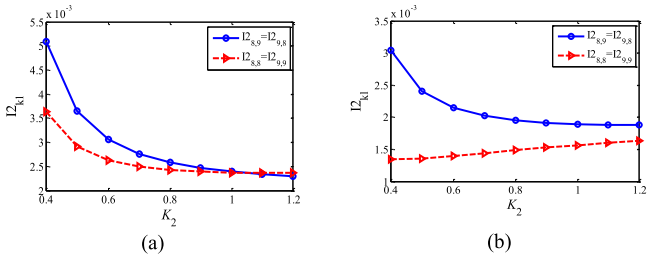

Fig. 11. Nonlinear interaction indices of dominant interacted modes when K_2 varies (a) dominant interacted modes of v_{o2d}, (b) dominant interacted modes of v_{o2q}.

(d), it can be noted that among all state variables, the load-stage output voltage v_{o2} has the largest interaction by K_1 and K_2. The variation of K_1 has the largest effect on the interacted modes $\lambda_{k=8,9,l=8,9}$ of the voltages v_{o2d} and v_{o2q}, which is the same as K_2.

In the two-stage boost inverter, the quality of the load-stage output voltage v_{o2} is tightly dependent on the source-stage

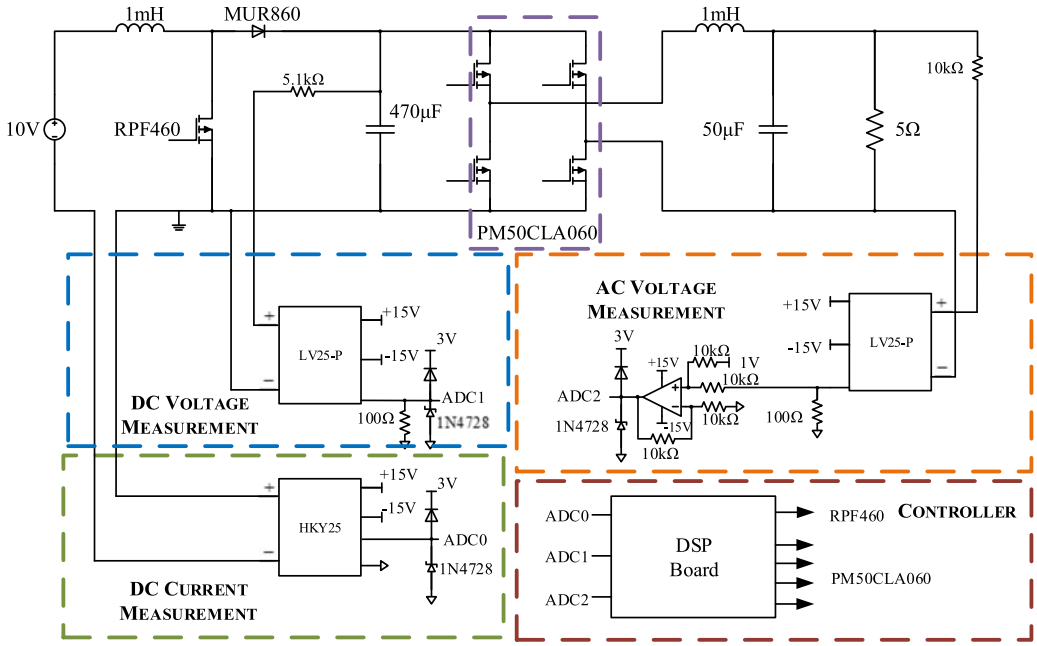

Fig. 12. Schematic of the two-stage boost inverter.

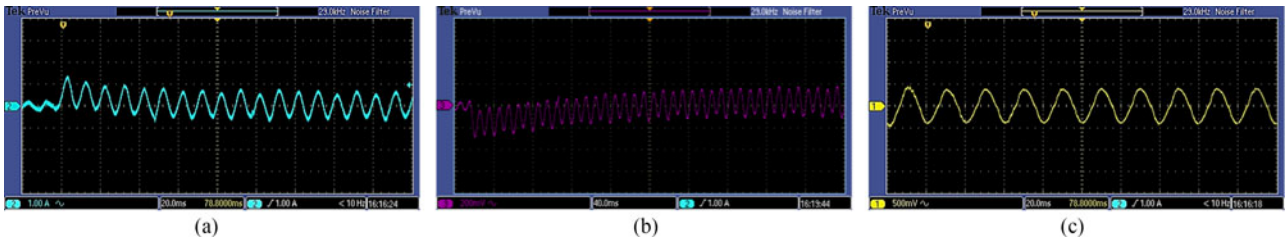

Fig. 13. Measured transient waveforms when $C_1 = 690\,\mu$F and $T_3 = 0.6 \times 10^{-3}$ for (a) inductor current of the source stage i_{L1}, (b) feedback output voltage of the source stage v_{o1}, and (c) feedback output voltage of the load stage v_{o2}.

output voltage v_{o1}. And then, the dynamical properties mainly depend on the control circuit if the power stage of the two-stage system is well designed. Therefore, the source-stage control parameters are the main concerned objects for the transient interaction in this two-stage system. In order to explore the variation of the dominant nonlinear interacted modes with the variation of system parameters, the variation of the interactions indices $I2^7_{k=8,9,l=8,9}$ and $I2^8_{k=8,9,l=8,9}$ with respect to K_1 and K_2 are displayed in Figs. 10 and 11, respectively. From Figs. 10(a) and 11(a), it can be explored that the nonlinear interaction of v_{o2d} is negative correlated with the variation of K_1 and K_2. In Figs. 10(b) and 11(b), it is shown that with the increase of K_1 or K_2, the interactions indices $I2_{8,9}$ and $I2_{9,8}$ decrease, whereas $I2_{8,8}$ and $I2_{9,9}$ maintain unchanged in v_{o2q}.

VI. Experiment Results

To show the validity of the above theoretical and numerical results, a prototype will be constructed as shown in Fig. 12. Some experimental results will be acquired to compare the transient behavior of the system under different values of C_1 and T_3. According to the equivalent principle of the control effect, one equivalent digital controller can be substituted for the above analog one. In this experiment, the circuit adopts digital control, RPF460 is the switch in the source-stage converter and PM50CLA060 is H-bridge in the load-stage inverter which are all regulated by TMS320F2812. The output voltage in the source stage and the load stage are sensed by two hall-effect voltage sensor (LV25-P). The inductor current in the source stage is sensed by a hall-effect current sensor (HKY25). These control parameters are the same as those parameters listed in Table II. The feedback gains of the output voltage in the source stage and load stage are $K_{s1} = 1/21$ and $K_{s2} = 1/40$, respectively.

To verify the validity of nonlinear modal analysis, the same sudden load jump as the theoretical analysis is performed in this experiment, i.e., the load abruptly changes from 15 to 5 Ω by using an air-break switch. Fig. 13 shows the measured transient waveforms of the inductor current i_{L1}, the feedback output voltage of the source stage $K_{s1}v_{o1}$ and the feedback output voltage of the load stage $K_{s2}v_{o2}$ when $C_1 = 690\,\mu$F and $T_3 = 0.6 \times 10^{-3}$. During this transient process, the measured settling times of i_{L1} and v_{o1} are 70 and 220 ms, respectively. Note that the transient response of $K_{s2}v_{o2}$ can be hardly observed from the measured waveforms, which is consistent with the simulation

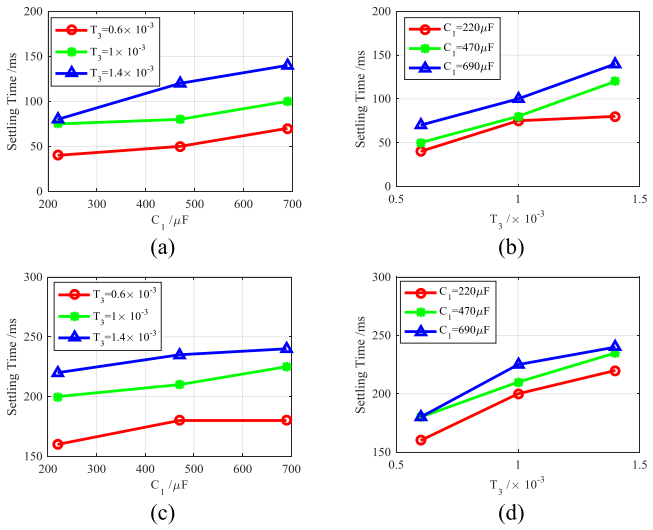

Fig. 14. Measured settling time with the variation of C_1 and T_3: (a) Settling time versus C_1 in i_{L1}. (b) Settling time versus T_3 in i_{L1}. (c) Settling time versus C_1 in v_{o1}. (d) Settling time versus T_3 in v_{o1}.

results in nonlinear modal analysis. Therefore, we will evaluate such transient performance as settling time in terms of i_{L1} and v_{o1}. The measured settling times of i_{L1} and v_{o1} under different values of C_1 and T_3 are shown in Fig. 14. It is clear from Fig. 14 that decreasing C_1 or T_3 can result in a shorter settling time, which just proves the conclusion in fundamental modal analysis. Furthermore, it is pointed out that the settling times of v_{o1} are always longer than ones of i_{L1}. The reason is just that based on the contribution factor, we can know that the dominant oscillation modes $\lambda_{8,9}$ have larger effect on v_{o1} rather than i_{L1} so that the oscillation process of v_{o1} will last much longer. Therefore, these experimental results verify that the nonlinear modal analysis is helpful in understanding the transient behavior of two-stage boost inverter.

VII. Conclusion

It has been shown that the existence of the "hidden" second-harmonic component results in a great deal of trouble in modeling and analysis. The observer-pattern modeling approach has been proposed to eliminate the effect of the time-variance from both the source stage and the load stage, and more significantly the hidden second harmonics from the nonlinear coupling effect between two subsystems have been unmasked. Furthermore, the nonlinear modal representation of the proposed observer-pattern model has been derived to characterize the substantial high-frequency dynamics of the transient process, and then the interaction mechanism of the transient behaviors has been uncovered by using the nonlinear modal analysis approach. First, the fundamental modal analysis has been performed to identify the correlation among fundamental modes, state variables, and system parameters. According to the two indices, i.e., nonlinear contribution factors and fundamental mode sensitivities, it follows that $\lambda_{1,2}$ and $\lambda_{3,4}$ are tightly correlated with the load stage, and $\lambda_{8,9}$ play the decisive role in the source stage. Moreover, decreasing the key parameters C_1 and T_3 will be beneficial to the dynamic response of each subsystem. Second, the second-order interacted modal analysis has been applied to exploring the dominant second-order interacted modes for crucial state variables and the relationship between modal interaction and system parameters. It is found that increasing the control parameters K_1 and K_2 are actually accompanied by the attenuation of nonlinear interaction. To sum up, these above results are helpful for the optimization of the transient performance qualitatively and quantitatively.

Appendix A

The Jacobian matrix A of this two-stage system is given as bottom of this page, where

$$A_{12}=\frac{\partial F_1}{\partial x_2}=-\frac{1}{L_1}+\frac{1}{L_1}d_1^e,\ A_{14}=\frac{\partial F_1}{\partial x_4}=\frac{1}{L_1}v_{o1}^e,$$
$$A_{21}=\frac{\partial F_2}{\partial x_1}=\frac{1}{C_1}-\frac{1}{C_1}d_1^e,\ A_{24}=\frac{\partial F_2}{\partial x_4}=-\frac{1}{C_1}i_{L1}^e,$$
$$A_{25}=\frac{\partial F_2}{\partial x_5}=-\frac{1}{2C_1}d_d^e(1-g_1^e),$$
$$A_{26}=\frac{\partial F_2}{\partial x_6}=-\frac{1}{2C_1}d_q^e(1-g_1^e),$$
$$A_{29}=\frac{\partial F_2}{\partial x_9}=-\frac{1}{2C_1}i_{L2d}^e(1-g_1^e),$$

$$\boldsymbol{A}=\left[\frac{\partial F_i}{\partial \boldsymbol{X}}\right]=\begin{bmatrix}
0 & A_{12} & 0 & A_{14} & 0 & 0 & 0 & 0 & 0 & 0 & 0 & 0\\
A_{21} & 0 & 0 & A_{24} & A_{25} & A_{26} & 0 & 0 & A_{29} & A_{210} & A_{211} & 0\\
A_{31} & A_{32} & 0 & A_{34} & A_{35} & A_{36} & 0 & 0 & A_{39} & A_{310} & A_{311} & 0\\
A_{41} & A_{42} & A_{43} & A_{44} & A_{45} & A_{46} & 0 & 0 & A_{49} & A_{410} & A_{411} & 0\\
0 & A_{52} & 0 & 0 & 0 & A_{56} & A_{57} & 0 & A_{59} & 0 & 0 & 0\\
0 & A_{62} & 0 & 0 & A_{65} & 0 & 0 & A_{68} & 0 & A_{610} & 0 & 0\\
0 & 0 & 0 & 0 & A_{75} & 0 & A_{77} & A_{78} & 0 & 0 & 0 & 0\\
0 & 0 & 0 & 0 & 0 & A_{86} & A_{87} & A_{88} & 0 & 0 & 0 & 0\\
0 & 0 & 0 & 0 & A_{95} & 0 & A_{97} & 0 & 0 & A_{910} & 0 & 0\\
0 & 0 & 0 & 0 & 0 & A_{106} & 0 & A_{108} & A_{109} & 0 & 0 & 0\\
0 & 0 & 0 & 0 & 0 & 0 & 0 & 0 & 0 & 0 & 0 & A_{1112}\\
0 & 0 & 0 & 0 & 0 & 0 & 0 & 0 & 0 & 0 & A_{1211} & 0
\end{bmatrix}$$

$$A_{210}=\frac{\partial F_2}{\partial x_{10}}=-\frac{1}{2C_1}i^e_{L2q}(1-g^e_1),$$
$$A_{211}=\frac{\partial F_2}{\partial x_{11}}=\frac{1}{2C_1}(i^e_{L2d}d^e_d+i^e_{L2q}d^e_q),$$
$$A_{31}=\frac{\partial F_3}{\partial x_1}=-\frac{K_1K_{s1}}{C_1}+\frac{K_1K_{s1}}{C_1}d^e_1$$
$$A_{32}=\frac{\partial F_3}{\partial x_2}=-\frac{K_1K_{s1}}{T_1}, A_{34}=\frac{\partial F_3}{\partial x_4}=\frac{K_1K_{s1}}{C_1}i^e_{L1},$$
$$A_{35}=\frac{\partial F_3}{\partial x_5}=\frac{K_1K_{s1}}{2C_1}d^e_d(1-g^e_1),$$
$$A_{36}=\frac{\partial F_3}{\partial x_6}=\frac{K_1K_{s1}}{2C_1}d^e_q(1-g^e_1),$$
$$A_{39}=\frac{\partial F_3}{\partial x_9}=\frac{K_1K_{s1}}{2C_1}i^e_{L2\mathrm{d}}(1-g^e_1),$$
$$A_{310}=\frac{\partial F_3}{\partial x_{10}}=\frac{K_1K_{s1}}{2C_1}i^e_{L2q}(1-g^e_1),$$
$$A_{311}=\frac{\partial F_3}{\partial x_{11}}=-\frac{K_1K_{s1}}{2C_1}(i^e_{L2d}d^e_d+i^e_{L2q}d^e_q),$$
$$A_{41}=\frac{\partial F_4}{\partial x_1}=\alpha_1+\alpha_4d^e_1,\ A_{42}=\frac{\partial F_4}{\partial x_2}=\alpha_2+\alpha_5d^e_1,$$
$$A_{43}=\frac{\partial F_4}{\partial x_3}=\alpha_3, A_{44}=\frac{\partial F_4}{\partial x_4}=\alpha_4i^e_{L1}+\alpha_5v^e_{o1},$$
$$A_{45}=\frac{\partial F_4}{\partial x_5}=\frac{\alpha_6}{2}d^e_d(1-g^e_1),$$
$$A_{46}=\frac{\partial F_4}{\partial x_6}=\frac{\alpha_6}{2}d^e_q(1-g^e_1),$$
$$A_{49}=\frac{\partial F_4}{\partial x_9}=\frac{\alpha_6}{2}i^e_{L2d}(1-g^e_1),$$
$$A_{410}=\frac{\partial F_4}{\partial x_{10}}=\frac{\alpha_6}{2}i^e_{L2q}(1-g^e_1),$$
$$A_{411}=\frac{\partial F_4}{\partial x_{11}}=-\frac{\alpha_6}{2}(i^e_{L2d}d^e_d+i^e_{L2q}d^e_q),$$
$$A_{52}=\frac{\partial F_5}{\partial x_2}=\frac{1}{L_2}d^e_d,\ A_{56}=\frac{\partial F_5}{\partial x_6}=\omega,$$
$$A_{57}=\frac{\partial F_5}{\partial x_7}=-\frac{1}{L_2},\ A_{59}=\frac{\partial F_5}{\partial x_9}=\frac{1}{L_2}v^e_{o1},$$
$$A_{62}=\frac{\partial F_6}{\partial x_2}=\frac{1}{L_2}d^e_q,\ A_{65}=\frac{\partial F_6}{\partial x_5}=-\omega,$$
$$A_{68}=\frac{\partial F_6}{\partial x_8}=-\frac{1}{L_2},\ A_{610}=\frac{\partial F_6}{\partial x_{10}}=\frac{1}{L_2}v^e_{o1},$$
$$A_{75}=\frac{\partial F_7}{\partial x_5}=\frac{1}{C_2},\ A_{77}=\frac{\partial F_7}{\partial x_7}=-\frac{1}{RC_2},$$
$$A_{78}=\frac{\partial F_7}{\partial x_8}=\omega,\ A_{86}=\frac{\partial F_8}{\partial x_6}=\frac{1}{C_2},$$
$$A_{87}=\frac{\partial F_8}{\partial x_7}=-\omega,\ A_{88}=\frac{\partial F_8}{\partial x_8}=-\frac{1}{RC_2},$$
$$A_{95}=\frac{\partial F_9}{\partial x_5}=\beta_1,\ A_{97}=\frac{\partial F_9}{\partial x_7}=\beta_2,$$
$$A_{910}=\frac{\partial F_9}{\partial x_{10}}=\omega,\ A_{106}=\frac{\partial F_{10}}{\partial x_6}=\beta_1,$$
$$A_{108}=\frac{\partial F_{10}}{\partial x_8}=\beta_2,\ A_{109}=\frac{\partial F_{10}}{\partial x_9}=-\omega,$$
$$A_{1112}=\frac{\partial F_{11}}{\partial x_{12}}=1,\ A_{1211}=\frac{\partial F_{12}}{\partial x_{11}}=-4\omega^2;$$

APPENDIX B

The Hessian sparse matrix (CSR format) $\boldsymbol{H}_i$ $(i=1,2,\ldots,12)$ for the two-stage boost inverter can be represented as

$$\boldsymbol{H}_1=[h_1,h_1]$$
$$\mathrm{I}\boldsymbol{H}_1=[0,0,1,1,2],$$
$$\mathrm{J}\boldsymbol{H}_1=[3,1]$$
$$\boldsymbol{H}_2=[h_2,h_2,h_3,h_4,h_3,h_5,h_3,h_6,h_3,h_7,h_4,h_5,h_6,h_7]$$
$$\mathrm{I}\boldsymbol{H}_2=[0,1,1,1,2,4,6,6,6,8,10,14],$$
$$\mathrm{J}\boldsymbol{H}_2=[3,0,8,10,9,10,4,10,5,10,4,5,8,9]$$
$$\boldsymbol{H}_3=[h_8,h_8,h_9,h_{10},h_9,h_{11},h_9,h_{12},h_9,h_{13},h_{10},h_{11},h_{12},h_{13}]$$
$$\mathrm{I}\boldsymbol{H}_3=[0,1,1,1,2,4,6,6,6,8,10,14],$$
$$\mathrm{J}\boldsymbol{H}_3=[3,0,8,10,9,10,4,10,5,10,4,5,8,9]$$
$$\boldsymbol{H}_4=[h_{14},h_{15},h_{14},h_{15},h_{16},h_{17},h_{16},h_{18},h_{16},h_{19},h_{16},h_{20},h_{17},h_{18},h_{19},h_{20}]$$
$$\mathrm{I}\boldsymbol{H}_4=[0,1,2,2,4,6,8,8,8,10,12,16],$$
$$\mathrm{J}\boldsymbol{H}_4=[3,3,0,1,8,10,9,10,4,10,5,10,4,5,8,9]$$
$$\boldsymbol{H}_5=[h_{21},h_{21}]\quad \boldsymbol{H}_6=[h_{21},h_{21}]$$
$$\mathrm{I}\boldsymbol{H}_5=[0,0,1,1,1,1,1,1,1,2]$$
$$\mathrm{I}\boldsymbol{H}_6=[0,0,1,1,1,1,1,1,1,1,2]$$
$$\mathrm{J}\boldsymbol{H}_5=[8,1]\quad \mathrm{J}\boldsymbol{H}_6=[9,1],$$
$$\boldsymbol{H}_7=\boldsymbol{0},\boldsymbol{H}_8=\boldsymbol{0},\boldsymbol{H}_9=\boldsymbol{0},\boldsymbol{H}_{10}=\boldsymbol{0},\boldsymbol{H}_{11}=\boldsymbol{0},\boldsymbol{H}_{12}=\boldsymbol{0}.$$

where

$$h_1=\frac{1}{L_1},\ h_2=-\frac{1}{C_1}, h_3=-\frac{1-g^e_1}{2C_1},$$
$$h_4=\frac{d^e_d}{2C_1}, h_5=\frac{d^e_q}{2C_1},\ h_6=\frac{i^e_{L2d}}{2C_1},$$
$$h_7=\frac{i^e_{L2q}}{2C_1},\ h_8=\frac{K_1K_{s1}}{C_1},$$
$$h_9=\frac{K_1K_{s1}(1-g^e_1)}{2C_1},\ h_{10}=-\frac{K_1K_{s1}d^e_d}{2C_1},$$
$$h_{11}=-\frac{K_1K_{s1}d^e_q}{2C_1},\ h_{12}=-\frac{K_1K_{s1}i^e_{L2d}}{2C_1},$$

$$h_{13} = -\frac{K_1 K_{s1} i^e_{L2q}}{2C_1},\ h_{14} = \frac{K_1 K_2 K_{s1}}{C_1 V_{m1}},$$
$$h_{15} = -\frac{K_2}{L_1 V_{m1}},\ h_{16} = \frac{K_1 K_2 K_{s1}(1-g^e_1)}{2C_1 V_{m1}},$$
$$h_{17} = -\frac{K_1 K_2 K_{s1} d^e_d}{2C_1 V_{m1}},\ h_{18} = -\frac{K_1 K_2 K_{s1} d^e_q}{2C_1 V_{m1}},$$
$$h_{19} = -\frac{K_1 K_2 K_{s1} i^e_{L2d}}{2C_1 V_{m1}},\ h_{20} = -\frac{K_1 K_2 K_{s1} i^e_{L2q}}{2C_1 V_{m1}},$$
$$h_{21} = \frac{1}{L_2}.$$

REFERENCES

[1] L. Zhang, X. B. Ruan, and X. Y. Ren, "Second-harmonic current reduction and dynamic performance improvement in the two-stage inverters: An output impedance perspective," *IEEE Trans. Ind. Electron.*, vol. 62, no. 1, pp. 394–404, Jan. 2015.

[2] M. Mirhosseini, J. Pou, and V. G. Agelidis, "Single- and two-stage inverter-based grid-connected photovoltaic power plants with ride-through capability under grid faults," *IEEE Trans. Sustain. Energy*, vol. 6, no. 3, pp. 1150–1159, Jul. 2015.

[3] P. Deivasundari, G. Uma, and R. Poovizhi, "Analysis and experimental verification of Hopf bifurcation in a solar photovoltaic powered hysteresis current-controlled cascaded-boost converter," *IET Power Electron.*, vol. 6, pp. 763–773, 2013.

[4] H. Zhang, W. Li, and H. Ding, "Nonlinear modal analysis of transient behavior in cascade DC-DC boost converters," *Int. J. Bifurcation Chaos*, vol. 27, 2017, Art. no. 1750140.

[5] M. E. Ahmed, M. Orabi, and O. M. AbdelRahim, "Two-stage micro-grid inverter with high-voltage gain for photovoltaic applications," *IET Power Electron.*, vol. 6, pp. 1812–1821, Nov. 2013.

[6] D. B. W. Abeywardana, B. Hredzak, and V. G. Agelidis, "An input current feedback method to mitigate the DC-side low-frequency ripple current in a single-phase boost inverter," *IEEE Trans. Power Electron.*, vol. 31, no. 6, pp. 4594–4603, 2016.

[7] A. A. Khan, H. Cha, H. F. Ahmed, J. Kim, and J. Cho, "A highly reliable and high-efficiency quasi single-stage buck–boost inverter," *IEEE Trans. Power Electron.*, vol. 32, no. 6, pp. 4185–4198, 2017.

[8] B. S. Zhang, A. Y. S. Lam, A. D. Dominguez-Garcia, and D. Tse, "An optimal and distributed method for voltage regulation in power distribution systems," *IEEE Trans. Power Syst.*, vol. 30, no. 4, pp. 1714–1726, Jul. 2015.

[9] X. Zhang, Q. C. Zhong, and W. L. Ming, "Stabilization of a cascaded DC converter system via adding a virtual adaptive parallel impedance to the input of the load converter," *IEEE Trans. Power Electron.*, vol. 31, no. 3, pp. 1826–1832, Mar. 2016.

[10] J. C. Tsai, C. L. Chen, Y. H. Lee, H. Y. Yang, M. S. Hsu, and K. H. Chen, "Modified hysteretic current control (MHCC) for improving transient response of boost converter," *IEEE Trans. Circuits Syst. I, Reg. Papers*, vol. 58, no. 8, pp. 1967–1979, Aug. 2011.

[11] G. R. Walker and P. C. Sernia, "Cascaded DC-DC converter connection of photovoltaic modules," *IEEE Trans. Power Electron.*, vol. 19, no. 4, pp. 1130–1139, Jul. 2004.

[12] H. Zhang, X. P. Yang, X. K. Ma, and F. Zheng, "Theoretical and experimental investigation of bidirectional Hopf bifurcations in cascade DC-DC buck converters," *Math. Comput. Simul.*, vol. 82, pp. 540–557, Dec. 2011.

[13] A. El Aroudi, D. Giaouris, H. H. C. Iu, and I. A. Hiskens, "A review on stability analysis methods for switching mode power converters," *IEEE J. Emerg. Sel. Top. Circuits Syst.*, vol. 5, no. 3, pp. 302–315, Sep. 2015.

[14] J. I. Y. Ota, Y. Shibano, N. Niimura, and H. Akagi, "A phase-shifted-PWM D-STATCOM using a modular multilevel cascade converter (SSBC)—part I: Modeling, analysis, and design of current control," *IEEE Trans. Ind. Appl.*, vol. 51, no. 1, pp. 279–288, Jan./Feb. 2015.

[15] J. I. Y. Ota, T. Sato, and H. Akagi, "Enhancement of performance, availability, and flexibility of a battery energy storage system based on a modular multilevel cascaded converter (MMCC-SSBC)," *IEEE Trans. Power Electron.*, vol. 31, no. 4, pp. 2791–2799, Apr. 2016.

[16] R. D. Middlebrook and S. Cuk, "A general unified approach to modelling switching-converter power stages," *Int. J. Electron.*, vol. 42, pp. 521–550, 1976.

[17] X. Zhang, X. Ruan, and C. K. Tse, "Impedance-based local stability criterion for DC distributed power systems," *IEEE Trans. Circuits Syst. I, Reg. Papers*, vol. 62, no. 3, pp. 916–925, Dec. 2015.

[18] R. Haroun, A. Cid-Pastor, A. El Aroudi, and L. Martinez-Salamero, "Synthesis of canonical elements for power processing in DC distribution systems using cascaded converters and sliding-mode control," *IEEE Trans. Power Electron.*, vol. 29, no. 3, pp. 1366–1381, Mar. 2014.

[19] J. Sun, "Impedance-based stability criterion for grid-connected inverters," *IEEE Trans. Power Electron.*, vol. 26, no. 11, pp. 3075–3078, Nov. 2011.

[20] Z. Liu, J. J. Liu, W. H. Bao, and Y. L. Zhao, "Infinity-norm of impedance-based stability criterion for three-phase AC distributed power systems with constant power loads," *IEEE Trans. Power Electron.*, vol. 30, no. 6, pp. 3030–3043, Jun. 2015.

[21] C. M. Wildrick, F. C. Lee, B. H. Cho, and B. C. Choi, "A method of defining the load impedance specification for a stable distributed power-system," *IEEE Trans. Power Electron.*, vol. 10, no. 3, pp. 280–285, May 1995.

[22] X. G. Feng, J. J. Liu, and F. C. Lee, "Impedance specifications for stable DC distributed power systems," *IEEE Trans. Power Electron.*, vol. 17, pp. 157–162, Mar. 2002.

[23] B. C. Choi, B. H. Cho, and S. S. Hong, "Dynamics and control of dc-to-dc converters driving other converters downstream," *IEEE Trans. Circuits Syst. I-Fundam. Theory Appl.*, vol. 46, no. 2, pp. 1240–1248, Oct. 1999.

[24] X. Li *et al.*, "Power management unit with its control for a three-phase fuel cell power system without large electrolytic capacitors," *IEEE Trans. Power Electron.*, vol. 26, no. 12, pp. 3766–3777, Dec. 2011.

[25] S. Jung, Y. Bae, S. Choi, and H. Kim, "A low cost utility interactive inverter for residential fuel cell generation," *IEEE Trans. Power Electron.*, vol. 22, no. 6, pp. 2293–2298, Nov. 2007.

[26] C. K. Tse and M. Li, "Design-oriented bifurcation analysis of power electronics systems," *Int. J. Bifurcation Chaos*, vol. 21, pp. 1523–1537, Jun. 2011.

[27] A. El Aroudi, D. Giaouris, H. H.-C. Iu, and I. A. Hiskens, "A review on stability analysis methods for switching mode power converters," *IEEE J. Emerg. Sel. Top. Circuits Syst.*, vol. 5, no. 3, pp. 302–315, Sep. 2015.

[28] A. El Aroudi, E. Rodriguez, M. Orabi, and E. Alarcon, "Modeling of switching frequency instabilities in buck-based DC-AC H-bridge inverters," *Int. J. Circuit Theory Appl.*, vol. 39, pp. 175–193, Feb. 2011.

[29] H. Zhang, C. Yi, and T. Wei, "Nonlinear modal analysis of transient interaction behaviors in SEPIC DC-DC converters," *IET Power Electron.*, vol. 10, pp. 1190–1199, 2017.

[30] M. Alfayyoumi, A. H. Nayfeh, and D. Borojevic, "Modeling and analysis of switching-mode DC-DC regulators," *Int. J. Bifurcation Chaos*, vol. 10, pp. 373–390, Feb. 2000.

[31] F. X. Wu, H. Wu, Z. X. Han, and D. Q. Gan, "Validation of power system non-linear modal analysis methods," *Elect. Power Syst. Res.*, vol. 77, pp. 1418–1424, Aug. 2007.

Hao Zhang (M'06) was born in Shaanxi, China, in 1973. He received the B.E. degree in industrial electrical automation from Xi'an University of Science & Technology, Xi'an, China, in 1996, the M.Sc. degree in detection technology and automatic equipment from Xi'an University of Technology, Xi'an, in 2002, and the Ph.D. (Hons.) degree in electrical engineering from Xi'an Jiaotong University, Xi'an, in 2005.

From December 2004 to June 2005, he was a Research Assistant with Hong Kong Polytechnic University, Hong Kong. Since 2007, he has been an Associate Professor in the School of Electrical Engineering, Xi'an Jiaotong University. During the academic year 2010–2011, he was a Visiting Professor at the Center for Power Electronics Systems, Virginia Tech. His research interests include power electronics and its application to renewable energy generation.

Weijie Li was born in Shaanxi, China, in 1989. He received the B.E. degree in industrial electrical automation from Northwest A&F University, Xianyang, China, in 2012, and the M.Sc. degree in electrical engineering from Xi'an Jiaotong University, Xi'an, China, in 2015.

He currently works at State Grid Tangshan Power Supply Branch Company, China. His research interests include complex behaviors of switching power converters.

Honghui Ding was born in Henan, China, in 1991. He received the B.S. degree in automation from Henan University of Science and Technology, Luoyang, China, in 2013 and the M.S. degree in electric engineering from Xi'an Jiaotong University, Xi'an, China, in 2017.

He currently works at State Grid Suqian Power Supply Branch Company, Taizhou, China. His research interests include modeling and transient analysis of multiport power converter.

Chuanzhi Yi received the B.S.E.E. degree in industrial electrical automation, in 2015, from Xi'an Jiaotong University, Xi'an, China, where he is currently working toward the M.Sc. degree in electrical engineering.

His research interests include modeling and optimizing of power converters for renewable energy applications.

Xiaojin Wan was born in Jiangsu, China, in 1991. He received the B.E. degree in industrial electrical automation from Dalian Maritime University, Dalian, China, in 2014, and the M.Sc. degree in electrical engineering from Xi'an Jiaotong University, Xi'an, China, in 2017.

He currently works at State Grid Taizhou Power Supply Branch Company, Taizhou, China. His research interests include modeling and transient analysis of power converters.